2D Triangle Splatting for Direct Differentiable Mesh Training

Supplementary Material

6. Detailed Proof of Equations

6.1. Render Normal from Depth

Given a rendered depth image d_j, we can infer a camera space normal image $\mathbf{n}'_j$ as follows. We first define:

$$\begin{aligned} \mathbf{D}_j &= [D_x, D_y]\,|_{\mathbf{P}_j} = \left[\frac{1}{d}\frac{\partial d}{\partial x}, \frac{1}{d}\frac{\partial d}{\partial y}\right]|_{\mathbf{P}_j}, \\ \mathbf{n}'_j &= \text{norm}\left(\left[n'_x, n'_y, n'_z\right]|_{\mathbf{P}_j}\right), \end{aligned} \tag{16}$$

where $\frac{\partial d}{\partial x}$ and $\frac{\partial d}{\partial y}$ are the depth gradient on the pixel $\mathbf{P}_j$ defined as the difference between the depth of adjacent pixels, which we calculate with a Scharr Filter. Then, we have:

$$\begin{aligned} n'_x &= \frac{WD_x}{2\tan(\frac{\text{FoV}_x}{2})}, \\ n'_y &= \frac{HD_y}{2\tan(\frac{\text{FoV}_y}{2})}, \\ n'_z &= 1 + D_x(x - \frac{W}{2} + 0.5) + D_y(y - \frac{H}{2} + 0.5), \end{aligned} \tag{17}$$

where W and H are the width and height of the image, x and y are the pixel coordinates.

6.2. Integration of Opacity

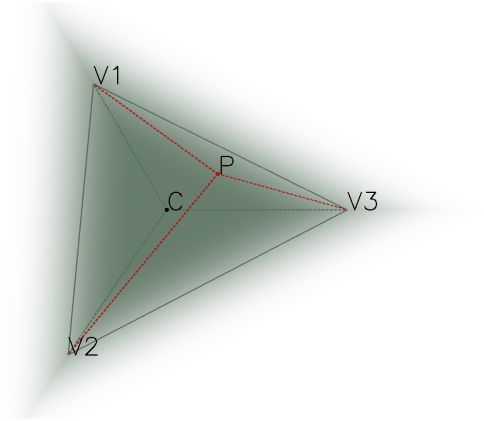

Figure 5. **Auxiliary Chart for the Integration of Opacity.**

We provide the detailed derivation of the integration of opacity over the triangle plane used in Equation 8 of the main paper.

$$I(\gamma) = \int_{\triangle} o_j \, dA = \int_{\triangle} O \cdot \exp(-\frac{1}{2}e_j^{2\gamma}) \, dA \tag{18}$$

We calculate the integration separately for the three subregions of the triangle divided by $\overline{CV_1}$, $\overline{CV_2}$, and $\overline{CV_3}$, where C is the barycenter, as shown in Figure 5. For the subregion enclosed by $\overline{CV_1}$ and $\overline{CV_2}$, we can transform the integration over area to integration over distance h to the edge $\overline{V_1V_2}$ since the opacity is constant at each point on a line parallel to $\overline{V_1V_2}$ in this subregion. So we have:

$$\begin{aligned} I_{\overline{CV_1}\vee\overline{CV_2}}(\gamma) &= \int_{-\infty}^{H} O \cdot \exp(-\frac{1}{2}e_{(h)}^{2\gamma}) \frac{H-h}{H} L_{\overline{V_1V_2}} dh \\ &= \int_{-\infty}^{H} O \cdot \exp(-\frac{1}{2}(1-\frac{h}{H})^{2\gamma})(1-\frac{h}{H}) L_{\overline{V_1V_2}} dh \\ &= \int_{0}^{\infty} \frac{1}{2} O \cdot H \cdot L_{\overline{V_1V_2}} \exp(-\frac{1}{2}x^{\gamma}) dx \\ &= \frac{2^{\frac{1}{\gamma}} O \cdot S}{3} \int_{0}^{\infty} \exp(-x^{\gamma}) dx \\ &= \frac{2^{\frac{1}{\gamma}} O \cdot S}{3} \frac{1}{\gamma} \Gamma(\frac{1}{\gamma}) \end{aligned} \tag{19}$$

where H is distance from C to $\overline{V_1V_2}$, $L_{\overline{V_1V_2}}$ is the length of $\overline{V_1V_2}$, and $S = \frac{3}{2}L_{\overline{V_1V_2}}H$ is the area of $\triangle_{V_1V_2V_3}$. The Euler's gamma function Γ is defined as:

$$\Gamma(x) = \int_0^{\infty} t^{x-1}e^{-t} dt.$$

Since the above integration is the same for all three subregions of the triangle plane, we have:

$$I(\gamma) = 3I_{\overline{CV_1}\vee\overline{CV_2}}(\gamma) = O \cdot S \cdot \frac{2^{\frac{1}{\gamma}}\Gamma(\frac{1}{\gamma})}{\gamma}. \tag{20}$$

7. Additional Experimental Results

7.1. Novel View Synthesis

We provide the detailed results of our experiments on each scene of the MipNeRF360 [2], NeRF-Synthetic [28], Tanks and Temples [23], and Deep Blending [15] datasets. The experiments are described in Section 4.2.

Figure 6 shows qualitative comparisons on the MipNeRF360 dataset. Tables 4, 5, and 6 show the quantitative results for the MipNeRF360, NeRF-Synthetic, Tanks and Temples, and Deep Blending datasets, respectively. Red indicates the best score in these tables while orange indicates the second best score.

Additional NVS Clarifications. We additionally report efficiency on Mip-NeRF360 and ablations on the NVS setting. All results in Table 8 use the same protocol as the main paper unless otherwise specified.

Figure 6. Visual comparison of the radiance field reconstruction between our method, 3DGS, and 2DGS on the MipNeRF360 dataset.

		Outdoor Scene					Indoor scene				
		bicycle	flowers	garden	stump	treehill	room	counter	kitchen	bonsai	mean
PSNR	M-Nerf360	24.37	21.73	26.98	26.40	22.87	31.63	29.55	32.23	33.46	27.69
	3DGS	24.71	21.09	26.63	26.45	22.33	30.50	29.07	31.13	32.26	27.24
	2DGS	24.82	20.99	26.91	26.41	22.52	30.86	28.45	30.62	31.64	27.03
	2DTS(Ours)	26.29	22.54	28.59	26.89	22.92	32.56	29.69	30.83	33.27	28.18
SSIM	M-Nerf360	0.685	0.583	0.813	0.744	0.632	0.913	0.894	0.920	0.941	0.792
	3DGS	0.729	0.571	0.834	0.762	0.627	0.922	0.913	0.922	0.926	0.797
	2DGS	0.731	0.573	0.845	0.764	0.630	0.918	0.908	0.927	0.940	0.804
	2DTS(Ours)	0.798	0.667	0.890	0.787	0.680	0.946	0.929	0.920	0.959	0.842
LPIPS	M-Nerf360	0.301	0.344	0.170	0.261	0.339	0.211	0.204	0.127	0.176	0.237
	3DGS	0.265	0.377	0.147	0.266	0.362	0.231	0.212	0.138	0.214	0.246
	2DGS	0.271	0.378	0.138	0.263	0.369	0.214	0.197	0.125	0.194	0.239
	2DTS(Ours)	0.211	0.290	0.107	0.244	0.335	0.229	0.206	0.150	0.192	0.218

Table 4. PSNR ↑, SSIM ↑, LPIPS ↓ scores for the MipNeRF360 [2] dataset.

		chair	drums	ficus	hotdog	lego	materials	mic	ship	mean
PSNR	Mip-NeRF	35.08	25.26	33.44	37.38	35.46	30.63	36.38	30.46	33.05
	3DGS	35.87	26.15	34.90	37.70	35.90	30.12	35.89	31.07	33.45
	2DGS	35.23	26.11	35.37	37.35	35.12	29.69	35.16	30.56	33.07
	2DTS(Ours)	35.57	26.23	35.86	37.69	36.03	30.19	35.80	30.71	33.51
SSIM	Mip-NeRF	0.980	0.934	0.981	0.982	0.978	0.959	0.991	0.885	0.961
	3DGS	0.988	0.955	0.987	0.985	0.983	0.962	0.992	0.907	0.970
	2DGS	0.985	0.954	0.988	0.984	0.980	0.958	0.991	0.904	0.968
	2DTS(Ours)	0.988	0.954	0.990	0.986	0.983	0.961	0.992	0.905	0.970
LPIPS	Mip-NeRF	0.041	0.104	0.045	0.038	0.053	0.054	0.024	0.177	0.067
	3DGS	0.012	0.036	0.012	0.020	0.015	0.033	0.006	0.105	0.030
	2DGS	0.015	0.040	0.012	0.023	0.020	0.039	0.007	0.110	0.033
	2DTS(Ours)	0.014	0.047	0.012	0.024	0.018	0.047	0.008	0.122	0.037

Table 5. PSNR ↑, SSIM ↑, LPIPS ↓ scores for the NeRF-Synthetic [28] dataset.

		Truck	Train	Dr Johnson	Playroom
PSNR	M-Nerf360	24.91	19.52	29.14	29.66
	3DGS	25.19	21.10	28.77	30.04
	2DGS	25.10	21.13	28.95	30.15
	2DTS(Ours)	25.40	21.38	28.98	29.76
SSIM	M-Nerf360	0.857	0.660	0.901	0.900
	3DGS	0.879	0.802	0.899	0.906
	2DGS	0.873	0.790	0.900	0.906
	2DTS(Ours)	0.886	0.820	0.906	0.909
LPIPS	M-Nerf360	0.159	0.354	0.237	0.252
	3DGS	0.148	0.218	0.244	0.241
	2DGS	0.173	0.251	0.256	0.257
	2DTS(Ours)	0.160	0.247	0.310	0.311

Table 6. PSNR ↑, SSIM ↑, LPIPS ↓ scores for the Tanks & Temples [23] and Deep Blending [15] datasets.

7.2. Mesh Reconstruction

We provide the detailed results of our experiments on each scene of the NeRF-Synthetic [28] and DTU [20] datasets. The experiments are described in Section 4.3. Figure 7 shows qualitative comparisons on the DTU dataset. Table 10 shows the results for the NeRF-Synthetic dataset. Table

	Training Time (min)↓	Memory (GB)↓	Rendering FPS↑
M-NeRF360	2735	0.38	0.08
3DGS	60	9.32	87
2DGS	98	2.60	32
2DTS (Ours)	48	2.63	50

Table 7. Training time, memory, and rendering FPS on Mip-NeRF360.

	PSNR↑	SSIM↑	LPIPS↓
Full Model	28.18	0.842	0.218
Vertex Color	28.39	0.844	0.209
Uniform Opacity	26.51	0.781	0.303
Pre-downsampled	27.32	0.814	0.246

Table 8. Ablations on the NVS setting of Mip-NeRF360. The main-paper setting uses face color and runtime bilinear downsampling.

11 shows the results for the DTU dataset.

For a more apples-to-apples comparison of rendering-based metrics, Table 9 reports results when all methods are rendered with the Kaolin renderer.

	NeRF-Synthetic				DTU			
	PSNR↑	SSIM↑	LPIPS↓	Count(K)↓	PSNR↑	SSIM↑	LPIPS↓	Count(K)↓
2DGS-Mesh	21.83	0.866	0.145	489	21.50	0.851	0.227	268
GOF-Mesh	22.13	0.876	0.136	501	22.25	0.869	0.193	1062
PGSR-Mesh	21.71	0.877	0.134	361	22.73	0.875	0.190	1047
Nvdiffrec	18.93	0.844	0.151	83	16.49	0.760	0.296	567
2DTS-Mesh (Ours)	25.60	0.909	0.118	73	24.22	0.874	0.212	265

Table 9. Rendering-based metrics with Kaolin for all methods.

		chair	drums	ficus	hotdog	lego	materials	mic	ship	mean
PSNR	2DGS-Mesh	25.64	19.73	18.01	25.91	22.72	18.83	22.13	21.64	21.83
	GOF-Mesh	25.73	19.01	18.86	25.43	23.98	20.68	21.72	21.61	22.13
	PGSR-Mesh	25.99	18.38	20.57	24.25	23.58	18.00	20.64	22.26	21.71
	Nvdiffrec	31.68	24.32	29.92	32.87	28.94	26.52	30.12	25.71	28.76
	2DTS-Mesh (Ours)	34.16	25.12	30.37	35.01	33.17	27.03	32.69	28.87	30.80
SSIM	2DGS-Mesh	0.898	0.844	0.876	0.920	0.852	0.847	0.915	0.772	0.866
	GOF-Mesh	0.906	0.845	0.886	0.933	0.879	0.865	0.916	0.782	0.876
	PGSR-Mesh	0.909	0.847	0.896	0.932	0.870	0.850	0.915	0.795	0.877
	Nvdiffrec	0.968	0.920	0.966	0.972	0.945	0.932	0.974	0.826	0.938
	2DTS-Mesh (Ours)	0.982	0.944	0.973	0.976	0.972	0.928	0.986	0.879	0.955
LPIPS	2DGS-Mesh	0.101	0.161	0.127	0.109	0.151	0.149	0.088	0.271	0.145
	GOF-Mesh	0.096	0.161	0.118	0.103	0.128	0.134	0.091	0.258	0.136
	PGSR-Mesh	0.090	0.159	0.102	0.098	0.136	0.148	0.090	0.253	0.134
	Nvdiffrec	0.045	0.092	0.050	0.063	0.065	0.089	0.042	0.194	0.080
	2DTS-Mesh (Ours)	0.025	0.067	0.044	0.063	0.038	0.100	0.025	0.165	0.066
CD(1e-3)	2DGS-Mesh	72.4	44.8	80.6	81.6	15.4	9.6	27.3	48.8	47.5
	GOF-Mesh	79.5	26.9	15.7	118.6	46.3	11.3	12.4	429.4	92.9
	PGSR-Mesh	113.1	28.1	23.9	122.0	34.8	17.2	19.7	35.1	49.2
	Nvdiffrec	57.4	32.5	15.4	27.2	26.7	18.0	9.8	393.0	72.5
	2DTS-Mesh (Ours)	23.0	25.8	8.5	14.6	4.7	9.8	11.8	124.2	27.8
Count(K)	2DGS-Mesh	355	480	119	414	758	485	235	1065	489
	GOF-Mesh	464	465	152	366	635	509	210	1205	501
	PGSR-Mesh	273	430	221	300	534	431	156	545	361
	Nvdiffrec	104	68	41	57	116	65	24	187	83
	2DTS-Mesh (Ours)	84	77	39	53	104	73	72	85	73

Table 10. PSNR ↑, SSIM ↑, LPIPS ↓ and Chamfer Distance (CD) ↓ scores for the NeRF-Synthetic [28] dataset. Face counts of the meshes are also reported.

Figure 7. Visual comparison of the mesh reconstruction between our method, 2DGS, GOF, PGSR, and Nvdiffrec on the DTU dataset.

		24	37	40	55	63	65	69	83	97	105	106	110	114	118	122	mean
PSNR	2DGS-Mesh	21.36	20.61	22.69	23.05	15.80	22.36	19.85	25.24	20.39	23.79	21.09	16.96	21.14	22.56	25.65	21.50
	GOF-Mesh	21.48	20.95	23.05	23.16	23.24	22.62	19.56	24.90	21.94	24.20	19.46	20.02	20.91	22.80	25.51	22.25
	PGSR-Mesh	22.12	21.19	23.43	23.17	25.31	22.88	19.92	24.10	21.57	23.63	21.98	19.11	23.73	22.25	26.52	22.73
	Nvdiffrec	23.34	23.75	24.70	25.42	29.83	26.00	23.59	28.77	24.66	27.34	23.86	24.55	25.67	26.13	30.77	25.89
	2DTS-Mesh (Ours)	30.68	28.31	30.85	30.57	32.31	29.13	25.03	29.62	27.69	29.81	26.49	26.44	29.45	30.13	33.27	29.32
SSIM	2DGS-Mesh	0.716	0.766	0.691	0.810	0.898	0.923	0.864	0.948	0.852	0.886	0.864	0.866	0.848	0.907	0.929	0.851
	GOF-Mesh	0.763	0.777	0.735	0.844	0.921	0.926	0.873	0.949	0.870	0.893	0.878	0.884	0.863	0.917	0.936	0.869
	PGSR-Mesh	0.777	0.793	0.739	0.846	0.932	0.931	0.878	0.949	0.876	0.895	0.888	0.881	0.877	0.922	0.940	0.875
	Nvdiffrec	0.703	0.762	0.658	0.833	0.928	0.925	0.888	0.957	0.879	0.896	0.865	0.902	0.837	0.921	0.948	0.860
	2DTS-Mesh (Ours)	0.925	0.918	0.913	0.958	0.965	0.961	0.915	0.970	0.935	0.946	0.947	0.937	0.936	0.962	0.971	0.944
LPIPS	2DGS-Mesh	0.374	0.231	0.371	0.217	0.164	0.161	0.278	0.121	0.231	0.218	0.234	0.221	0.262	0.182	0.139	0.227
	GOF-Mesh	0.280	0.206	0.307	0.169	0.132	0.143	0.252	0.113	0.192	0.195	0.201	0.200	0.229	0.160	0.119	0.193
	PGSR-Mesh	0.277	0.203	0.316	0.174	0.118	0.141	0.245	0.114	0.188	0.191	0.194	0.198	0.218	0.159	0.117	0.190
	Nvdiffrec	0.404	0.260	0.415	0.226	0.150	0.159	0.260	0.107	0.213	0.220	0.247	0.208	0.263	0.176	0.118	0.228
	2DTS-Mesh (Ours)	0.141	0.135	0.209	0.131	0.089	0.104	0.249	0.095	0.162	0.157	0.148	0.177	0.153	0.127	0.094	0.145
CD	2DGS-Mesh	0.603	0.825	0.332	0.351	0.956	0.871	0.798	1.330	1.188	0.675	0.654	2.206	0.393	0.676	0.473	0.819
	GOF-Mesh	0.496	0.836	0.461	0.387	1.409	0.812	0.809	1.274	1.317	0.665	0.733	1.291	0.486	0.692	0.506	0.812
	PGSR-Mesh	0.367	0.544	0.400	0.336	0.779	0.576	0.488	1.080	0.635	0.585	0.463	0.548	0.304	0.369	0.340	0.521
	Nvdiffrec	2.436	1.701	2.438	1.351	2.573	1.733	1.568	1.822	2.042	1.480	1.649	3.464	1.732	1.451	1.248	1.907
	2DTS-Mesh (Ours)	0.458	0.593	0.360	0.395	0.632	0.752	0.591	0.848	1.197	0.373	0.482	0.764	0.349	0.401	0.361	0.570
Count(K)	2DGS-Mesh	492	453	332	257	260	349	304	207	182	216	229	175	140	212	205	268
	GOF-Mesh	1526	1823	1278	954	1722	1302	1129	792	806	852	850	756	551	788	798	1062
	PGSR-Mesh	1475	1509	1320	958	1579	1371	1183	847	705	869	930	678	568	875	834	1047
	Nvdiffrec	2056	1007	1037	418	615	534	483	155	429	243	346	257	392	322	208	567
	2DTS-Mesh (Ours)	535	508	717	531	183	180	53	67	118	215	209	71	270	161	162	265

Table 11. PSNR ↑, SSIM ↑, LPIPS ↓ and Chamfer Distance (CD) ↓ scores for the DTU [20] dataset. Face counts of the meshes are also reported.